







Unconventional gapless semiconductor in an extended martini lattice in covalent honeycomb materials

Tomonari Mizoguchi ^{*}, Yanlin Gao , Mina Maruyama , Yasuhiro Hatsugai , and Susumu Okada 
Department of Physics, Graduate School of Pure and Applied Sciences, University of Tsukuba, 1-1-1 Tennodai, Tsukuba, Ibaraki 305-8571, Japan

 (Received 1 September 2022; revised 17 February 2023; accepted 21 February 2023; published 13 March 2023)

We study characteristic electronic structures in an extended martini lattice model and propose its materialization in π -electron networks constructed by designated chemisorption on graphene and silicene. By investigating the minimal tight-binding model, we reveal rich electronic structures tuned by the ratio of hopping parameters, ranging from the band insulator to the unconventional gapless semiconductor. Remarkably, the unconventional gapless semiconductor is characterized by a flat band at the Fermi level. Further, the density functional theory calculations for candidate materials reveal that the characteristic electronic structures can be realized by designated chemisorption or chemical substitution on graphene and silicene, and that the electronic structure near the Fermi level is tunable by the choice of the atomic species of adsorbed atoms. Our results open the way to search exotic electronic structures and their functionalities induced by an extended martini lattice.

DOI: [10.1103/PhysRevB.107.L121301](https://doi.org/10.1103/PhysRevB.107.L121301)

Introduction. Exotic electronic structures are a source of rich phenomena in solid-state physics. In particular, the density of states (DOS) near the Fermi energy is one of the key quantities for the determination of physical properties, such as phase transitions and the response to external electric and magnetic fields. In this regard, bands with constant energy in the entire Brillouin zone, called flat bands, are of particular interest because they provide diverging DOS, which implies instability. Indeed, when flat bands are present near the Fermi energy, various correlation-induced phases such as ferromagnetism [1,2] and superconductivity [3–7] are predicted to be realized. Also, it may induce a structural deformation (i.e., the Peierls instability).

Recently, the search for flat-band materials has become active [8–10]. Among various routes for realizing flat bands, electronic structure engineering in two-dimensional materials with π -electron networks, such as graphene [11–15] and silicene [16–18], has attracted considerable attention. One of the most prominent findings along this line is the emergence of strongly correlated physics and superconductivity in twisted bilayer graphene [19–22], which originates from twist-induced flat bands, or moiré flat bands, appearing in designated twist angles called magic angles [23]. Another promising method for electronic structure engineering is fabricating superstructures [24] by making holes or chemical substitutions/adsorptions. π electrons do not have in-plane anisotropy, so their electronic structures are largely dominated by the geometrical structures of lattices they live on. This fact leads to a clear guiding principle for realizing flat bands, namely, to arrange the π -electron network such that it is equivalent to the famous flat-band lattice models. For instance, the flat bands originating from a kagomelike network

appear in graphene with periodic holes [25,26] and hydrocarbon networks containing sp^2 and sp^3 carbons [27–29] (i.e., the covalent organic framework). In this Letter, we propose a characteristic π -electron network hosting a flat band, which we refer to as an extended martini lattice [Fig. 1(a)]. The network consists of corner sharing triangles (solid and dashed red bonds), which is equivalent to a kagome lattice, and Y-shaped units (blue bonds) centered at the downward triangles. Without downward triangles, (i.e., the dashed red bonds), the lattice is called a martini lattice [30–34], which belongs to a class of flat-band lattices called a partial line graph [30,31]. Hence, the extension we consider here refers to the existence of downward triangles.

We first elucidate the characteristic band structures in an extended martini lattice by employing a minimal tight-binding model. We find that the electronic structure strongly depends on the ratio between two hopping parameters. In particular, when the ratio exceeds a critical value, the lattice system becomes an unconventional gapless semiconductor where a flat band is at the conduction band edge or the valence band edge. We further show, based on density functional theory, that an extended martini lattice can be realized by partial chemisorption of graphene and silicene. In those materials, the flat bands acquire a finite dispersion, resulting in carrier doping to the flat bands accompanied by ferromagnetic ordering. Remarkably, the electronic structure near the band edge can be controlled by species of adsorbed atoms, which will open a way to search for exotic properties and functionalities in these systems.

Robust flat band in an extended martini lattice model. The main target of this Letter is the extended martini lattice model, shown in Fig. 1(a). There are four sublattices per unit cell. Thus, in a tight-binding model for spinless, single-orbital fermions, the Bloch Hamiltonian $H_{\mathbf{k}}$ has the form of a 4×4 matrix. The explicit form of $H_{\mathbf{k}}$ is shown in the Supplemental

^{*}mizoguchi@rhodia.ph.tsukuba.ac.jp

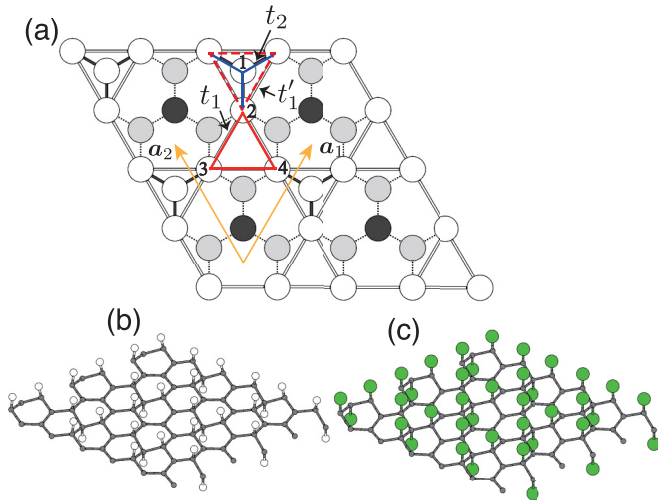


FIG. 1. (a) Schematic views of extended martini networks derived from hexagonal covalent networks of C and Si. White and gray circles denote C and Si without and with adsorbates, respectively. The adsorbates are adsorbed on gray atomic sites in (a) from the top and bottom of the layer. Orange arrows represent the lattice vectors $\mathbf{a}_1 = a_0(\frac{1}{2}, \frac{\sqrt{3}}{2})$ and $\mathbf{a}_2 = a_0(-\frac{1}{2}, \frac{\sqrt{3}}{2})$, where a_0 is the length of the unit cell edge. The on-site potential V is introduced on sublattice 1. Optimized geometric structures of (b) partially hydrogenated graphene, and (c) partially fluorinated graphene. Gray, green, and white spheres denote C, F, and H atoms, respectively.

Material [35]. There are four parameters: t_1 , t_1' , t_2 , and V . Note that a conventional martini lattice model, which belongs to the partial line graph [30], corresponds to the case of $t_1' = V = 0$.

We elucidate that an exact flat band appears for any parameter, using the wisdom of linear algebra [36–41]. To begin with, we introduce three column vectors: $\boldsymbol{\psi}_{k,1} = (0, 1, 1, 1)^T$ and $\boldsymbol{\psi}_{k,2} = (0, 1, e^{-ik \cdot \mathbf{a}_1}, e^{-ik \cdot \mathbf{a}_2})^T$, and $\boldsymbol{\psi}_{k,3} = (1, 0, 0, 0)^T$ [42]. We additionally introduce a 4×3 matrix, $\Psi_k = (\boldsymbol{\psi}_{k,1} \ \boldsymbol{\psi}_{k,2} \ \boldsymbol{\psi}_{k,3})$. Its Hermitian conjugate Ψ_k^\dagger is a 3×4 matrix. It follows that, for any \mathbf{k} , there exists a four-component vector $\boldsymbol{\varphi}_k$ that satisfies $\Psi_k^\dagger \boldsymbol{\varphi}_k = \mathbf{0}$. In other words, $\boldsymbol{\varphi}_k$ belongs to the kernel of the linear map represented by Ψ_k^\dagger . Its explicit form can be easily obtained for generic \mathbf{k} ,

$$\boldsymbol{\varphi}_k = \frac{1}{\mathcal{N}_k} (0, e^{ik \cdot \mathbf{a}_2} - e^{ik \cdot \mathbf{a}_1}, 1 - e^{ik \cdot \mathbf{a}_2}, e^{ik \cdot \mathbf{a}_1} - 1)^T, \quad (1)$$

with \mathcal{N}_k being the normalization constant. Note that $\boldsymbol{\varphi}_k$ has a vanishing amplitude at sublattice 1. The remaining finite components on sublattices 2–4 are identical to those of the flat-band wave functions of a kagome lattice. Note also that $\boldsymbol{\varphi}_k$ becomes a zero vector at $\mathbf{k} = (0, 0)$ (i.e., Γ point), namely, $\boldsymbol{\varphi}_k$ is singular at this point. We will address the implication of this fact later.

A key property for obtaining the flat band is that H_k can be expressed by the matrices introduced above,

$$H_k = \Psi_k \begin{pmatrix} t_1 & 0 & 0 \\ 0 & t_1' & t_2 \\ 0 & t_2 & V - \varepsilon^{\text{FB}} \end{pmatrix} \Psi_k^\dagger + \varepsilon^{\text{FB}} I_4, \quad (2)$$

where $\varepsilon^{\text{FB}} = -(t_1 + t_1')$. Recalling that $\Psi_k^\dagger \boldsymbol{\varphi}_k = \mathbf{0}$ holds, we find $\boldsymbol{\varphi}_k$ is the eigenvector of H_k with the eigenenergy being a \mathbf{k} -independent value ε^{FB} .

Band structures of a tight-binding model. We discuss the characteristics of the entire band structure, including exact flat bands. In what follows, we focus on the case where $t_1 = t_1' = -1$ and $V = 0$, leaving an analysis of the generic parameters to the Supplemental Material [35]. In Fig. 2, we plot the band structures for several values of t_2/t_1 . We see that, in all panels, an exact flat band with the energy being ε^{FB} indeed exists. At the Γ point, quadratic band touching between the flat band and the dispersive band occurs. Such a band touching is ubiquitous in various flat-band models [38,43–48]. Band touching can be accounted for by the singularity of $\boldsymbol{\varphi}_k$ which we have addressed before. In fact, at the Γ point, $\boldsymbol{\psi}_{k,1} = \boldsymbol{\psi}_{k,2}$ holds, which results in an increase of the dimension of the kernel of Ψ_k^\dagger from 1 to 2. Hence, only at this specific point, there are two eigenstates with an eigenenergy $\varepsilon = \varepsilon^{\text{FB}}$, resulting in quadratic band touching [38,40,41,49–51].

Besides these parameter-independent features, we also see in Fig. 2 that varying t_2/t_1 causes a change in the entire band structure. Since the target materials are half filled, we will focus on this case in the following discussions. For $0 < t_2/t_1 < 2$ [Figs. 2(a)–2(c)], the system is a conventional band insulator, where two dispersive bands are completely filled. Interestingly, at the fine-tuned parameter corresponding to Fig. 2(b), the flat band is doubly degenerate. At $t_2/t_1 = 2$ [Fig. 2(d)], triple band touching occurs at the Γ point, around which the dispersive bands exhibit a linear dispersion. The analytic derivation of this critical value is shown in the Supplemental Material [35]. For $t_2/t_1 > 2$ [Fig. 2(e)], the system becomes an unconventional gapless semiconductor, where the top of the valence band touches the empty flat band. The Fermi level is right at the flat band, meaning that the DOS is divergently large. This will be a source of exotic physical properties, as we will discuss later. Notably, the extended martini model provides a natural realization of an unconventional gapless semiconductor at half filling, which is distinct from other typical flat-band lattices. To be specific, the flat band is at the top or bottom of the entire bands for a line-graph lattice, while the flat band is half filled in Lieb-type lattices. Hence, neither of them realizes an unconventional gapless semiconductor. Considering that the blue bonds are shorter than the red bonds in Fig. 1(a), it is reasonable to assume that $|t_2| \gg |t_1| = |t_1'|$ holds when implementing this structure by π -electron networks. We thus focus on the unconventional gapless state [Fig. 2(e)] in the following discussions.

Two types of unconventional gapless semiconductor. Before proceeding to the material realizations, we note that the sign of t_1 is essential in determining the actual electronic state [52]. The schematic figure of the electronic structures around the Fermi level for $|t_2| > 2|t_1|$ is shown in Fig. 3. For $t_1 < 0$, which is the case of Fig. 2(e), the dispersive band touching the flat band is convex downward and is completely filled, whereas the flat band is completely empty. We refer to this case as type I [Fig. 3(a)]. Meanwhile, for $t_1 > 0$, the entire band structure is obtained by flipping the sign of the eigenenergies of those for $t_1 < 0$. As a result, we find that the dispersive band touching the flat band is convex upward

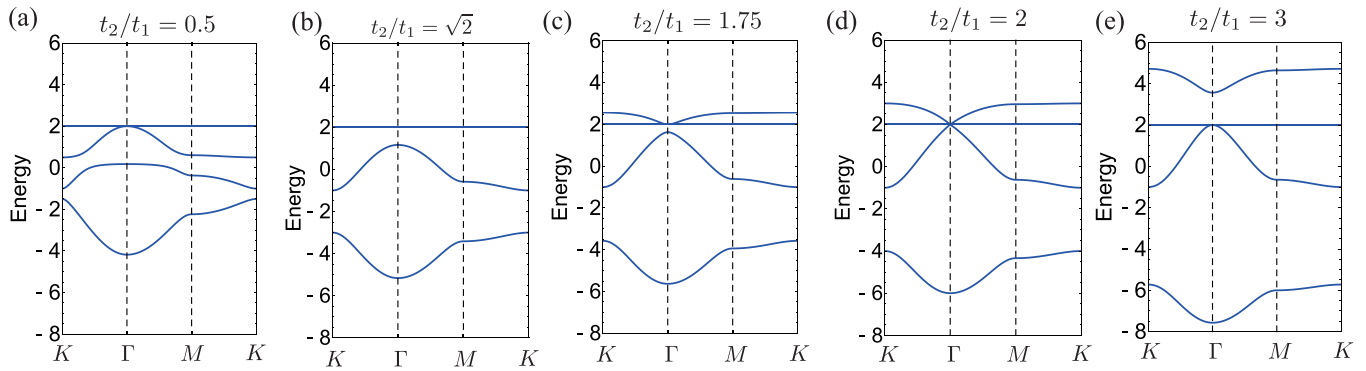


FIG. 2. Band structure for a tight-binding model along the high-symmetry lines in the Brillouin zone. The high-symmetry points are $\Gamma = (0, 0)$, $K = (\frac{4\pi}{3a_0}, 0)$, and $M = (\frac{\pi}{a_0}, \frac{\sqrt{3}\pi}{3a_0})$. We fix $t_1 = t'_1 = -1$, $V = 0$, and vary t_2/t_1 whose value is shown at the top of each panel.

and is completely empty; instead, the flat band right below the dispersive band is completely filled. We refer to this case as type II [Fig. 3(b)]. In fact, both types are feasible by the choice of mother materials and adatoms, as we shall discuss below.

Material design of an extended martini lattice. We now argue the material realization of the extended martini model. The geometric and electronic structures of realistic martini structures derived from graphene and silicene are investigated using the density functional theory [53,54]. See Supplemental Material [35] (and references therein) for details of the calculation methods.

Covalent honeycomb networks of C and Si are plausible starting materials to design an extended martini lattice because a corresponding network is obtained by partially thinning out the π electrons by adsorption or chemical substitution. Here, we focus on the adsorption on graphene, leaving the results for silicene for the Supplemental Material [35]. Figure 1(a) shows the schematic views of the possible structure of an extended martini lattice derived from a honeycomb C network. An extended martini lattice can be found in Fig. 1(a) as downward three-pointed stars comprising white circles by adsorbing or substituting four of eight atomic sites forming upward three-pointed stars in each 2×2 lateral unit cell by foreign atoms. The chemisorption of H onto graphene and silicene effectively removes π electrons on H-terminated C atomic sites, leading to an extended martini lattice of π

electrons on the partially H-adsorbed graphene [C-H in Fig. 1(b)]. Partial fluorination of graphene also effectively causes an extended martini lattice [C-F in Fig. 1(c)]. The optimized lattice parameters of extended martini networks of C-H and C-F are 5.04 and 5.04 Å, respectively, which are slightly longer than that of graphene, because the chemisorption on four of eight atomic sites per cell leads to sp^3 bonds. In addition to the adsorption, the substitution of C by B and N atoms can substantially modulate the π electron environment on the honeycomb networks, so that the in-plane heterostructures of three-pointed stars of C and B/N are possible candidates for an extended martini lattice. We argue the details of this case in the Supplemental Material [35].

Figures 4(a) and 4(b) show the electronic band structure of an extended martini lattice derived from the honeycomb networks of C. The extended martini systems of C-H and C-F are semiconductors where the two branches just below and above the Fermi level in the majority- and the minority-spin states, respectively, possess a characteristic dispersion relation: One of the two is less dispersive and the other has dispersion with a substantial width. Furthermore, these two branches degenerate at the Γ point. These characteristic dispersion relations are the same as those obtained by the tight-binding approximation, indicating that these networks are an extended martini lattice derived from graphene by atom adsorption. The adsorbate species on graphene can control the band structure attributed to the extended martini lattice. The flat band emerges in the lower branches and upper branches of two branches for extended martini lattices of C-F and C-H, respectively. Comparing these with the tight-binding model, we find that C-F corresponds to type I in Fig. 3(a), while C-H corresponds to type II in Fig. 3(b). These facts imply that the constituent elements of honeycomb networks and the adsorbates can control a sign of the effective electron transfer between the next-nearest π electrons (i.e., t_1 and t'_1), allowing further band edge engineering in these graphene derivatives.

In an extended martini lattice derived from graphene, a long-range wave-function overlap and incomplete π termination by adsorbates lead to a small but finite band dispersion in the flat-band state. The calculated bandwidths of the flat-band states are 0.46 and 0.23 eV for extended martini lattices of C-H and C-F, respectively. This small but finite bandwidth leads to partial occupation that causes a large Fermi level

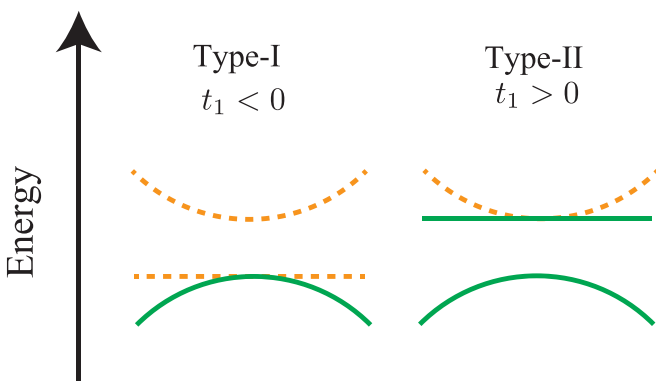


FIG. 3. Schematic figure of the band structure around the Fermi levels for $|t_2| \gg |t_1|$ for $t_1 < 0$ (i.e., type I) and $t_1 > 0$ (i.e., type II). The solid green (dashed orange) bands are filled (empty).

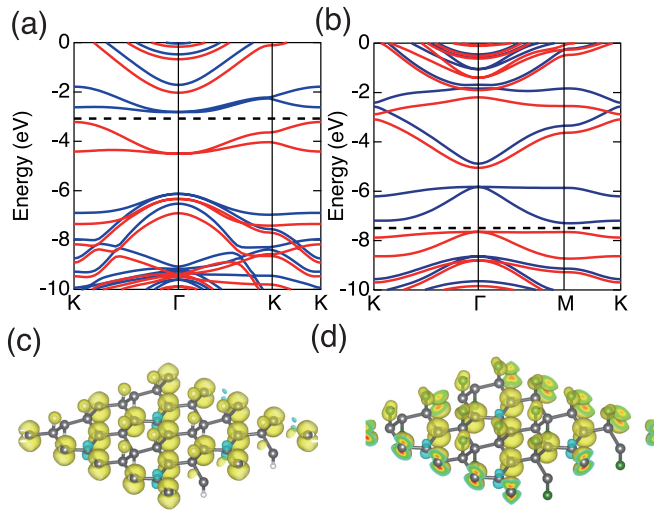


FIG. 4. Upper row: Electronic structures of (a) partially hydrogenated graphene, and (b) partially fluorinated graphene. The energies are measured from the vacuum level. Red and blue curves denote the energy band for majority and minority states, respectively. The horizontal dotted line indicates the Fermi level. Lower row: Iso-surfaces of polarized electron spin, $\Delta\rho(\vec{r}) = \rho(\vec{r})_{mj} - \rho(\vec{r})_{mn}$, where $\rho(\vec{r})_{mj}$ and $\rho(\vec{r})_{mn}$ are charge densities of majority- and minority-spin states, respectively, of (c) partially hydrogenated graphene, and (d) partially fluorinated graphene. Yellow and blue isosurfaces denote the electron accumulation and depression, respectively. Gray, green, and white spheres denote C, F, and H atoms, respectively.

instability. Extended martini networks of C-H and C-F exhibit spin polarization as shown in Figs. 4(a) and 4(b), respectively. The majority and minority bands associated with the martini flat-band state shift downward and upward, respectively, owing to spin polarization. The polarized spin is primarily distributed on the three edges of a three-pointed star of bare C atoms [Fig. 4(c) for C-H and Fig. 4(d) for C-F]. The distribution corresponds to the wave function of the martini bands at Γ and the Fermi level. Namely, the flat-band wave function of Eq. (1) has a vanishing amplitude at sublattice 1. The number of polarized electrons is 2 per 2×2 unit cell for both C-H and C-F, corresponding to $0.15\mu_B/\text{\AA}^2$. Therefore, these facts indicate that the partial hydrogenation or fluorination of graphene (as well as the partial hydrogenation of silicene [35]) are magnetic materials whose magnetization is attributed to itinerant π electrons on atomic layer materials. In contrast, C/BN heterostructures obtained by B/N substitution do not exhibit spin polarization, owing to the substantial bandwidth of the flat-band states. The calculated bandwidths of the flat-band states are 1 eV or wider [35].

Summary and discussions. We have investigated the characteristic electronic structures in an extended martini lattice model and its materialization in partially chemisorbed graphene and silicene. The analytic treatment of the tight-binding model reveals that an unconventional gapless semiconductor with an exact flat band at the Fermi level is realized when $|t_2| > 2|t_1|$ (for $t_1 = t'_1$). Depending on the sign of t_1 and t'_1 , the gapless semiconductor is classified as type I, with a

completely empty flat band, and type II, with a completely filled flat band. In actual materials, the types can be tuned by the species of the adsorbed atoms.

We close this Letter by addressing possible future problems and intriguing functionalities of extended martini materials. First, regarding the candidate materials design, there can be rich combinations of mother compounds, adatoms, and substituents. The choices of them determine the tight-binding parameters, as well as the characters out of our idealized models such as the bandwidth of nearly flat bands, which may enable the realization of various band structures in Fig. 2. In addition to monolayer materials, our scheme of electronic state engineering is also applicable to surface systems, such as a (111) surface of silicon or diamond [55,56]. An extensive materials search and electronic-structure analysis by density functional theory calculation will be an interesting future problem. Experimentally, recent developments on the scanning tunneling microscope technique have enabled single-atom manipulation [57–59], which will open the door to fabricating extended martini materials by a periodic alignment of adatoms. Another class of candidate materials is metal-organic frameworks and covalent organic frameworks. There, a three-dimensional analog of the extended martini network, which corresponds to a pyrochlore lattice with one additional site per downward tetrahedron, may also be pursued.

Second, as for the functionality due to spin polarization, it is expected that an electronic state such as that shown in Figs. 4(a) and 4(b) can be utilized for spin-filtered transport. Furthermore, when the spin polarization is weak such that the flat band of the majority spin is partially filled, the interplay between the flat-band state of majority spins and the mobile holes of the minority spins will give rise to exotic many-body states. Studying such situations will be an intriguing future problem.

Finally, if one can suppress the spin polarization and retain a nonmagnetic unconventional gapless semiconductor, the sharply varying DOS around the Fermi level can be a source of large thermoelectric responses [60–62]. Further, very recent theoretical studies have revealed that the quadratic band touching between the flat and the dispersive bands gives rise to an unconventional quantum geometric tensor, which anomalously affects various fundamental quantities such as a magnetic-field response [63,64] and a superfluid weight [65–67]. The extended martini materials will serve as suitable platforms for studying these phenomena.

Acknowledgments. The authors thank the Japan Science and Technology Agency, Core Research for Evolutionary Science and Technology (JST-CREST Grants No. JPMJCR1715, No. JPMJCR19T1, and No. JPMJCR20B5) and the Japan Society for the Promotion of Science, Grants-in-Aid for Scientific Research (JSPS KAKENHI Grants No. JP21H05233, No. JP21H05232, No. JP21K14484, No. JP20K22323, No. JP20H00316, No. JP20H02080, No. JP20K05253, No. JP20K14371, and No. JP20H05664), and the Joint Research Program on Zero-Emission Energy Research, Institute of Advanced Energy, Kyoto University. A part of the calculations was performed on an NEC SX-Aurora TSUBASA at the Cybermedia Center at Osaka University.

- [1] A. Mielke, *J. Phys. A: Math. Gen.* **24**, 3311 (1991).
- [2] H. Tasaki, *Phys. Rev. Lett.* **69**, 1608 (1992).
- [3] M. Imada and M. Kohno, *Phys. Rev. Lett.* **84**, 143 (2000).
- [4] T. T. Heikkilä, N. B. Kopnin, and G. E. Volovik, *JETP Lett.* **94**, 233 (2011).
- [5] S. Peotta and P. Törmä, *Nat. Commun.* **6**, 8944 (2015).
- [6] H. Aoki, *J. Supercond. Novel Magn.* **33**, 2341 (2020).
- [7] V. Peri, Z.-D. Song, B. A. Bernevig, and S. D. Huber, *Phys. Rev. Lett.* **126**, 027002 (2021).
- [8] D. Călugăru, A. Chew, L. Elcoro, Y. Xu, N. Regnault, Z.-D. Song, and B. A. Bernevig, *Nat. Phys.* **18**, 185 (2022).
- [9] N. Regnault, Y. Xu, M.-R. Li, D.-S. Ma, M. Jovanovic, A. Yazdani, S. S. P. Parkin, C. Felser, L. M. Schoop, N. P. Ong, R. J. Cava, L. Elcoro, Z.-D. Song, and B. A. Bernevig, *Nature (London)* **603**, 824 (2022).
- [10] C. S. Chiu, A. N. Carroll, N. Regnault, and A. A. Houck, *Phys. Rev. Res.* **4**, 023063 (2022).
- [11] P. R. Wallace, *Phys. Rev.* **71**, 622 (1947).
- [12] K. S. Novoselov, A. K. Geim, S. V. Morozov, D. Jiang, Y. Zhang, S. V. Dubonos, I. V. Grigorieva, and A. A. Firsov, *Science* **306**, 666 (2004).
- [13] K. S. Novoselov, A. K. Geim, S. V. Morozov, D. Jiang, M. I. Katsnelson, I. V. Grigorieva, S. V. Dubonos, and A. A. Firsov, *Nature (London)* **438**, 197 (2005).
- [14] A. K. Geim and K. S. Novoselov, *Nat. Mater.* **6**, 183 (2007).
- [15] A. H. Castro Neto, F. Guinea, N. M. R. Peres, K. S. Novoselov, and A. K. Geim, *Rev. Mod. Phys.* **81**, 109 (2009).
- [16] J. C. Garcia, D. B. de Lima, L. V. C. Assali, and J. F. Justo, *J. Phys. Chem. C* **115**, 13242 (2011).
- [17] P. Vogt, P. De Padova, C. Quaresima, J. Avila, E. Frantzeskakis, M. C. Asensio, A. Resta, B. Ealet, and G. Le Lay, *Phys. Rev. Lett.* **108**, 155501 (2012).
- [18] A. Fleurence, R. Friedlein, T. Ozaki, H. Kawai, Y. Wang, and Y. Yamada-Takamura, *Phys. Rev. Lett.* **108**, 245501 (2012).
- [19] Y. Cao, V. Fatemi, S. Fang, K. Watanabe, T. Taniguchi, E. Kaxiras, and P. Jarillo-Herrero, *Nature (London)* **556**, 43 (2018).
- [20] Y. Cao, V. Fatemi, A. Demir, S. Fang, S. L. Tomarken, J. Y. Luo, J. D. Sanchez-Yamagishi, K. Watanabe, T. Taniguchi, E. Kaxiras, R. C. Ashoori, and P. Jarillo-Herrero, *Nature (London)* **556**, 80 (2018).
- [21] M. Yankowitz, S. Chen, H. Polshyn, Y. Zhang, K. Watanabe, T. Taniguchi, D. Graf, A. F. Young, and C. R. Dean, *Science* **363**, 1059 (2019).
- [22] J. M. Park, Y. Cao, K. Watanabe, T. Taniguchi, and P. Jarillo-Herrero, *Nature (London)* **590**, 249 (2021).
- [23] G. Tarnopolsky, A. J. Kruchkov, and A. Vishwanath, *Phys. Rev. Lett.* **122**, 106405 (2019).
- [24] N. Shima and H. Aoki, *Phys. Rev. Lett.* **71**, 4389 (1993).
- [25] M. Maruyama, N. T. Cuong, and S. Okada, *Carbon* **109**, 755 (2016).
- [26] M. Maruyama and S. Okada, *Carbon* **125**, 530 (2017).
- [27] J.-y. Sorimachi and S. Okada, *Phys. Rev. B* **96**, 024103 (2017).
- [28] Y. Fujii, M. Maruyama, K. Wakabayashi, K. Nakada, and S. Okada, *J. Phys. Soc. Jpn.* **87**, 034704 (2018).
- [29] Y. Fujii, M. Maruyama, and S. Okada, *Jpn. J. Appl. Phys.* **57**, 125203 (2018).
- [30] S. Miyahara, K. Kubo, H. Ono, Y. Shimomura, and N. Furukawa, *J. Phys. Soc. Jpn.* **74**, 1918 (2005).
- [31] K. Kubo, C. Hotta, S. Miyahara, and N. Furukawa, *Phys. B: Condens. Matter* **378-380**, 273 (2006).
- [32] C. R. Scullard, *Phys. Rev. E* **73**, 016107 (2006).
- [33] P. A. McClarty, M. Haque, A. Sen, and J. Richter, *Phys. Rev. B* **102**, 224303 (2020).
- [34] D. Matsumoto, T. Mizoguchi, and Y. Hatsugai, *J. Phys. Soc. Jpn.* **92**, 034705 (2023).
- [35] See Supplemental Material at <http://link.aps.org/supplemental/10.1103/PhysRevB.107.L121301> for the detailed numerical and analytical calculations on the tight-binding model, the details of the DFT calculation, and the additional DFT results on partially hydrogenated silicene and BCN heterostructures, which includes Refs. [68–71].
- [36] Y. Hatsugai and I. Maruyama, *Europhys. Lett.* **95**, 20003 (2011).
- [37] Y. Hatsugai, K. Shiraishi, and H. Aoki, *New J. Phys.* **17**, 025009 (2015).
- [38] T. Mizoguchi and Y. Hatsugai, *Europhys. Lett.* **127**, 47001 (2019).
- [39] T. Mizoguchi, M. Maruyama, S. Okada, and Y. Hatsugai, *Phys. Rev. Mater.* **3**, 114201 (2019).
- [40] T. Mizoguchi and Y. Hatsugai, *Phys. Rev. B* **101**, 235125 (2020).
- [41] T. Mizoguchi, Y. Kuno, and Y. Hatsugai, *Phys. Rev. B* **104**, 035161 (2021).
- [42] Note that $\psi_{k,1}$ and $\psi_{k,3}$ are actually k independent.
- [43] D. L. Bergman, C. Wu, and L. Balents, *Phys. Rev. B* **78**, 125104 (2008).
- [44] T. Bilitewski and R. Moessner, *Phys. Rev. B* **98**, 235109 (2018).
- [45] J.-W. Rhim and B.-J. Yang, *Phys. Rev. B* **99**, 045107 (2019).
- [46] Y. Hwang, J.-W. Rhim, and B.-J. Yang, *Phys. Rev. B* **104**, L081104 (2021).
- [47] Y. Hwang, J.-W. Rhim, and B.-J. Yang, *Phys. Rev. B* **104**, 085144 (2021).
- [48] A. Graf and F. Piéchon, *Phys. Rev. B* **104**, 195128 (2021).
- [49] Y. Hatsugai, *Ann. Phys.* **435**, 168453 (2021).
- [50] T. Mizoguchi, Y. Kuno, and Y. Hatsugai, *Prog. Theor. Exp. Phys.* (2022) 023102.
- [51] T. Kuroda, T. Mizoguchi, H. Araki, and Y. Hatsugai, *J. Phys. Soc. Jpn.* **91**, 044703 (2022).
- [52] It is worth noting that the sign of t_2 is irrelevant to the band structure. We argue this point in the Supplemental Material [35].
- [53] P. Hohenberg and W. Kohn, *Phys. Rev.* **136**, B864 (1964).
- [54] W. Kohn and L. J. Sham, *Phys. Rev.* **140**, A1133 (1965).
- [55] S. Okada, K. Shiraishi, and A. Oshiyama, *Phys. Rev. Lett.* **90**, 026803 (2003).
- [56] J. Zhou, Q. Sun, and P. Jena, *Phys. Rev. Lett.* **119**, 046403 (2017).
- [57] I.-W. Lyo and P. Avouris, *Science* **253**, 173 (1991).
- [58] Y. Sugimoto, P. Jelinek, P. Pou, M. Abe, S. Morita, R. Perez, and O. Custance, *Phys. Rev. Lett.* **98**, 106104 (2007).
- [59] Y. Sugimoto, P. Pou, O. Custance, P. Jelinek, M. Abe, R. Perez, and S. Morita, *Science* **322**, 413 (2008).
- [60] A. Sommerfeld and H. Bethe, *Elektronentheorie der Metalle, Handbuch der Physik* (Springer, Berlin, 1933), Vol. 24/2.
- [61] N. F. Mott and H. Jones, *The Theory of the Properties of Metals and Alloys* (Dover, New York, 1936).
- [62] J. M. Luttinger, *Phys. Rev.* **135**, A1505 (1964).
- [63] J.-W. Rhim, K. Kim, and B.-J. Yang, *Nature (London)* **584**, 59 (2020).

- [64] Y. Hwang, J.-W. Rhim, and B.-J. Yang, *Nat. Commun.* **12**, 6433 (2021).
- [65] M. Iskin, *Phys. Rev. A* **97**, 033625 (2018).
- [66] X. Hu, T. Hyart, D. I. Pikulin, and E. Rossi, *Phys. Rev. Lett.* **123**, 237002 (2019).
- [67] K.-E. Huhtinen, J. Herzog-Arbeitman, A. Chew, B. A. Bernevig, and P. Törmä, *Phys. Rev. B* **106**, 014518 (2022).
- [68] Y., K. Iwata, and K. Terakura, *Appl. Surf. Sci.* **169-170**, 11 (2001).
- [69] A simulation tool for atom technology (STATE), <https://state-doc.readthedocs.io/en/latest/index.html>.
- [70] J. P. Perdew, K. Burke, and M. Ernzerhof, *Phys. Rev. Lett.* **77**, 3865 (1996).
- [71] D. Vanderbilt, *Phys. Rev. B* **41**, 7892 (1990).